Ion Channels: From Atomic Resolution Physiology to Functional Genomics: Novartis Foundation Symposium 245. Volume 245
Edited by Gregory Bock and Jamie A. Goode
 ISBN: 0-470-84375-6

ION CHANNELS:
FROM ATOMIC RESOLUTION PHYSIOLOGY TO FUNCTIONAL GENOMICS

The Novartis Foundation is an international scientific and educational charity (UK Registered Charity No. 313574). Known until September 1997 as the Ciba Foundation, it was established in 1947 by the CIBA company of Basle, which merged with Sandoz in 1996, to form Novartis. The Foundation operates independently in London under English trust law. It was formally opened on 22 June 1949.

The Foundation promotes the study and general knowledge of science and in particular encourages international co-operation in scientific research. To this end, it organizes internationally acclaimed meetings (typically eight symposia and allied open meetings and 15–20 discussion meetings each year) and publishes eight books per year featuring the presented papers and discussions from the symposia. Although primarily an operational rather than a grant-making foundation, it awards bursaries to young scientists to attend the symposia and afterwards work with one of the other participants.

The Foundation's headquarters at 41 Portland Place, London W1B 1BN, provide library facilities, open to graduates in science and allied disciplines. Media relations are fostered by regular press conferences and by articles prepared by the Foundation's Science Writer in Residence. The Foundation offers accommodation and meeting facilities to visiting scientists and their societies.

Information on all Foundation activities can be found at
http://www.novartisfound.org.uk

Novartis Foundation Symposium 245

ION CHANNELS: FROM ATOMIC RESOLUTION PHYSIOLOGY TO FUNCTIONAL GENOMICS

2002

JOHN WILEY & SONS, LTD

Published in 2002 by John Wiley & Sons Ltd,
Baffins Lane, Chichester,
West Sussex PO19 1UD, England

National 01243 779777
International (+44) 1243 779777
e-mail (for orders and customer service enquiries): cs-books@wiley.co.uk
Visit our Home Page on http://www.wiley.co.uk
or http://www.wiley.com

Other Wiley Editorial Offices

John Wiley & Sons, Inc., 605 Third Avenue,
New York, NY 10158-0012, USA

WILEY-VCH Verlag GmbH, Pappelallee 3,
D-69469 Weinheim, Germany

John Wiley & Sons Australia, Ltd, 33 Park Road,
Milton, Queensland 4064, Australia

John Wiley & Sons (Asia) Pte Ltd, 2 Clementi Loop #02-01,
Jin Xing Distripark, Singapore 129809

John Wiley & Sons (Canada) Ltd, 22 Worcester Road,
Rexdale, Ontario M9W 1L1, Canada

Novartis Foundation Symposium 245
ix+273 pages, 67 figures, 11 tables

British Library Cataloguing in Publication Data

A catalogue record for this book is available from the British Library

ISBN 0 470 84375 6

Typeset in 10½ on 12½ pt Garamond by Dobbie Typesetting Limited, Tavistock, Devon.
Printed and bound in Great Britain by Biddles Ltd, Guildford and King's Lynn.
This book is printed on acid-free paper responsibly manufactured from sustainable forestry,
in which at least two trees are planted for each one used for paper production.

Contents

Symposium on Ion channels: from atomic resolution physiology to functional genomics, held at the Novartis Foundation, London, 12–14 June 2001

Editors: Gregory Bock (Organizer) and Jamie A. Goode

This symposium is based on a proposal made by Mark Sansom

Mark S. P. Sansom Introduction: stretching the envelope in structure–function studies of ion channels 1

Nigel Unwin Structure of the acetylcholine-gated channel 5
Discussion 15

Katjuša Brejc, Willem J. van Dijk, August B. Smit and **Titia K. Sixma** The 2.7 Å structure of AChBP, homologue of the ligand-binding domain of the nicotinic acetylcholine receptor 22
Discussion 29

Alok K. Mitra, Gang Ren, Vijay S. Reddy, Anchi Cheng and **Alexandrine Froger** The architecture of a water-selective pore in the lipid bilayer visualized by electron crystallography in vitreous ice 33
Discussion 46

Dax Fu, Andrew Libson and **Robert Stroud** The structure of GlpF, a glycerol conducting channel 51
Discussion 61

Mark S. P. Sansom, Peter Bond, Oliver Beckstein, Philip C. Biggin, José Faraldo-Gómez, Richard J. Law, George Patargias and **D. Peter Tieleman** Water in ion channels and pores — simulation studies 66
Discussion 79

Benoit Roux What can be deduced about the structure of Shaker from available data? 84
Discussion 101

Stefano Garofoli, Gennady Miloshevsky, Vladimir L. Dorman and **Peter C. Jordan** Permeation energetics in a model potassium channel 109
Discussion 122

Jacqueline M. Gulbis The β subunit of K_v1 channels: voltage-gated enzyme or safety switch? 127
Discussion 142

E. Perozo, L. G. Cuello, D. M. Cortes, Y.- S. Liu and **P. Sompornpisut** EPR approaches to ion channel structure and function 146
Discussion 158

General discussion I From structure to channel physiology 165

Senyon Choe, Susan Cushman, Kent A. Baker and **Paul Pfaffinger** Excitability is mediated by the T1 domain of the voltage-gated potassium channel 169
Discussion 175

Diane M. Papazian, William R. Silverman, Meng-chin A. Lin, Seema K. Tiwari-Woodruff and **Chih-Yung Tang** Structural organization of the voltage sensor in voltage-dependent potassium channels 178
Discussion 190

Michelle M. Pirruccello, Nikolaus Grigorieff and **Joseph A. Mindell** Electron diffraction of a bacterial ClC-type chloride channel 193
Discussion 203

John B. C. Findlay and **Michael A. Harrison** A protein chemical approach to channel structure and function: the proton channel of the vacuolar H^+-ATPase 207
Discussion 218

Anthony Auerbach Acetylcholine receptors, between closed and open 223
Discussion 234

David B. Sattelle, Emmanuel Culetto, Marta Grauso, Valérie Raymond, Christopher Franks and **Paula Towers** Functional genomics of ionotropic acetylcholine receptors in *Caenorhabditis elegans* and *Drosophila melanogaster* 240
Discussion 257

Final general discussion 261

Index of contributors 265

Subject index 267

Participants

Frances Ashcroft (*Chair*) University of Oxford, University Laboratory of Physiology, Parks Road, Oxford OX1 3PT, UK

Anthony Auerbach Department of Physiology and Biophysics, State University of New York, 324 Cary Hall, South Campus, Buffalo, NY 14214, USA

Senyon Choe The Salk Institute for Biological Studies, 10010 North Torrey Pines Road, La Jolla, CA 92037-1099, USA

Pierre-Jean Corringer Neurobiologie Moléculaire, Institut Pasteur, 25, rue du Dr Roux, F-75015 Paris, France

Declan Doyle Laboratory of Molecular Biophysics, The Rex Richards Building, Department of Biochemistry, University of Oxford, South Parks Road, Oxford OX1 3QU, UK

John Findlay School of Biochemistry & Molecular Biology, Faculty of Biological Sciences, University of Leeds, Leeds, LS2 9JT, UK

Dax Fu Biology Department, Building 463, 50 Bell Avenue, Brookhaven National Laboratory, Upton, NY 11973, USA

Jacqueline Gulbis The Walter and Eliza Hall Institute of Medical Research, Post Office, The Royal Melbourne Hospital, Melbourne, VIC 3050, Australia

Peter Jordan Department of Chemistry MS-015, Brandeis University, PO Box 549110, Waltham, MA 02454-9110, USA

Jeremy Lambert Department of Pharmacology and Neuroscience, University of Dundee, Dundee DD1 4HN, UK

Alistair Mathie Biophysics Group, Blackett Laboratory, Imperial College, Prince Consort Road, London SW7 2BZ, UK

Keith Miller Harvard Medical School, Massachusetts General Hospital, Department of Anaesthesia, Fruit Street, Edwards 505, Boston, MA 02114, USA

Joseph Mindell Department of Biochemistry, Brandeis University, 415 South Street, Waltham, MA 02454-9110, USA

Alok Mitra Department of Cell Biology, The Scripps Research Institute, Mail Stop MB21, 10550 North Torrey Pines Rd, La Jolla, CA 92037, USA

Diane Papazian Department of Physiology, UCLA School of Medicine, 405 Hilgard Avenue, Box 951751, Los Angeles, CA 90095-1361, USA

Eduardo Perozo Department of Molecular Physiology and Biological Physics, University of Virginia, PO Box 800736, Charlottesville, VA 22908-0736, USA

Chris Poll Novartis Horsham Research Centre, Wimblehurst Road, Horsham RH12 5AB, UK

Benoit Roux Department of Biochemistry, Weill Medical College of Cornell University, 1300 York Ave, Box #63, Room W-220, New York, NY 10021, USA

Mark Sansom Laboratory of Molecular Biophysics, Department of Biochemistry, Rex Richards Building, University of Oxford, South Parks Road, Oxford OX1 3QU, UK

David Sattelle MRC Functional Genetics Unit, Department of Human Anatomy and Genetics, University of Oxford, South Parks Road, Oxford OX1 3QX, UK

Tilman Schirmer University of Basel Biozentrum, Abteilung Strukturbiologie, Klingelbergstrasse 70, Basel, CH-4056, Switzerland

Hildgund Schrempf Universität Osnabrück, Fachbereich Biologie/Chemie, Barbarastr. 11, D-49069 Osnabrück, Germany

Titia Sixma Netherlands Cancer Institute, Division of Molecular Carcinogenesis, Plesmanlaan 121, 1066 CX Amsterdam, The Netherlands

Kenton Swartz Molecular Physiology and Biophysics Unit, NINDS Building 36, Room 2C19, 36 Convent Drive, MSC 4066, Bethesda, MD 20892-4066, USA

Peter Tieleman Department of Biological Sciences, University of Calgary, 2500 University Drive NW, Calgary, Alberta, Canada T2N 1N4

Nigel Unwin MRC Laboratory of Molecular Biology, Hills Road, Cambridge CB2 2QH, UK

Bonnie A. Wallace School of Crystallography, Birkbeck College, University of London, Malet Street, London WC1E 7HX, UK

Su Li Novartis Horsham Research Centre, Wimblehurst Road, Horsham RH12 5AB, UK

John Westwick Novartis Horsham Research Centre, Wimblehurst Road, Horsham RH12 5AB, UK

Ion Channels: From Atomic Resolution Physiology to Functional Genomics: Novartis Foundation Symposium 245. Volume 245
Edited by Gregory Bock and Jamie A. Goode
 ISBN: 0-470-84375-6

Permeation energetics in a model potassium channel

Stefano Garofoli, Gennady Miloshevsky, Vladimir L. Dorman and Peter C. Jordan[1]

Department of Chemistry, MS-015, Brandeis University, PO Box 549110, Waltham, MA 02454-9110, USA

Abstract. Known structures of selective ion channels share a common property: a narrow constriction, presumably crucial for ionic discrimination. This region can be fairly long, imposing single file motion on waters and ion(s). We apply the semi-microscopic Monte Carlo approach to study permeation in the KcsA channel, decomposing energetics into a three-step process: cation dehydration; ion transfer into a uniform low ε dielectric; and transfer from the uniform dielectric into the channel. The influence of individual channel structural features is separately assessed. The aqueous cavity has only a modest stabilizing effect on nearby ions in the filter. Ionic solvation in the filter reflects the combined influence of the single file waters, the binding pockets' carbonyls, the α helices directed at the cavity and the negative residues near the extracellular surface of the channel; no one feature dominates. At all sites along the permeation pathway there is substantial discrimination favouring K^+ over Na^+; conversely, there is little discrimination among the larger alkali cations. Selectivity for K^+ over Na^+ appears due to the inability of the filter's carbonyl oxygens to ideally coordinate Na^+.

2002 Ion channels — from atomic resolution physiology to functional genomics. Wiley, Chichester (Novartis Foundation Symposium 245) p 109–126

Until recently theoretical study of ionic interaction with ion channel proteins was either based on structural speculations or limited to considering the model system gramicidin (see Roux & Karplus 1994). The situation is now dramatically different. Four distinct selective channel systems have been solved to atomic level resolution: a K^+ channel from *Streptomyces lividans* (KcsA; Doyle et al 1998), a stretch-activated channel from *Mycobacterium tuberculosis* (Tb-McsL; Chang et al 1998), human red cell aquaporin 1 (AQP1; Murata et al 2000) and the *Escherichia coli* glycerol facilitator (GlpF; Fu et al 2000). All share a common feature, a constricted region where the transported species must lose much of its surrounding water and pass in close proximity to the channel protein. In KcsA the constriction is

[1]This paper was presented at the symposium by Peter Jordan, to whom correspondence should be addressed.

visible from the X-ray structure and is associated with a single file domain like that in gramicidin (Wallace 1999), but substantially shorter, some 10–15 Å long. A similar feature may be integral to the function of AQP1 (Murata et al 2000).

The structure of KcsA confirmed many electrophysiological inferences, investing kinetic models of the multi-ion permeation pathway (Hille & Schwartz 1978, Neyton & Miller 1988) with structural reality (Doyle et al 1998). It also revealed some unexpected architectural details: the carbonyl binding pockets, the mid-channel aqueous cavity and the α helices aimed at the cavity. The AQP1 structure, with α helices pointed at the constriction, rationalizes how this protein forms water channels and simultaneously blocks proton transport.

Nonetheless, questions remain. In KcsA, what creates essentially barrier-less free energy profiles for permeant ion transport, i.e. why are K^+ channel conductances so high? What accounts for essentially insurmountable energetic obstructions to the flow of similar competing species, i.e. why is the K^+/Na^+ permeability ratio so high? How do individual structural features affect permeation energetics? Which features simply lead to superposable static fields and which induce major dielectric reorientation?

This chapter examines these issues, describing the effect of individual structural features on the permeation free energy profile, and suggesting reasons for certain aspects of channel design. We extend the approach to compare permeation energetics among the alkali cations, emphasizing the importance of hydration energetics.

Modelling ion channels

Many theoretical approaches illuminate structure–function relationships in ion channels. Gramicidin has been their proving ground (Roux & Karplus 1994, Dorman et al 1996, Woolf & Roux 1997, Chiu et al 1991, Jakobsson & Chiu 1987). Using the X-ray structure of KcsA as a guide, insight has been gained from electrostatic analysis (Roux & MacKinnon 1999), Brownian dynamics (BD) (Chung et al 1999) and molecular dynamics (MD) (Åqvist & Luzhkov 2000, Shrivastava & Sansom 2000, Bernèche & Roux 2000, Guidoni et al 2000, Biggin et al 2001). In MD, the computational models hew closely to the known structure and provide a wealth of information. Among the simulational results are: a model for the permeation duty cycle (Åqvist & Luzhkov 2000); evidence for the permeant ions' role in structurally stabilizing the channel (Shrivastava & Sansom 2000); a detailed picture for the functional permeating assembly (Bernèche & Roux 2000); identification of a possible secondary influence of the oriented α helices (Guidoni et al 2000); and a novel hypothesis for the origin of K^+/Na^+ selectivity (Biggin et al 2001). In contrast, both BD and electrostatic studies are mesoscopic in nature, necessarily partially idealized. The transmembrane aqueous pathway is a

continuum fluid with high permittivity, approaching or equal to that of bulk water, even though water in narrow constrictions must be ordered and non-permittive (Partenskii & Jordan 1992, Partenskii et al 1994). BD successfully reproduced gross aspects of transport kinetics (Chung et al 1999). The Roux & MacKinnon (1999) study provided a basis for the cavity's ability to preferentially solvate monovalent cations.

Our perspective on KcsA is somewhat different. We treat prescribed structural features that we believe critical for the energetics of ion transfer from water (Dorman et al 1996, 1999). These define an exactly soluble, computationally efficient statistical mechanical problem. The model, illustrated in Fig. 1, incorporates a few mobile, reorientable features (the ion[s], the single file waters in the channel, and the carbonyls forming the binding pockets); the remainder (the cavity, the oriented α helices and the negative residues) are, for computational convenience, treated as fixed background charges, although this restriction can be lifted. The bulk water domains are continua with high dielectric constants, for computational simplicity chosen as infinite. The cavity is treated in two ways: as a high ε continuum or by incorporating explicit cavity waters, $\sim$20 additional

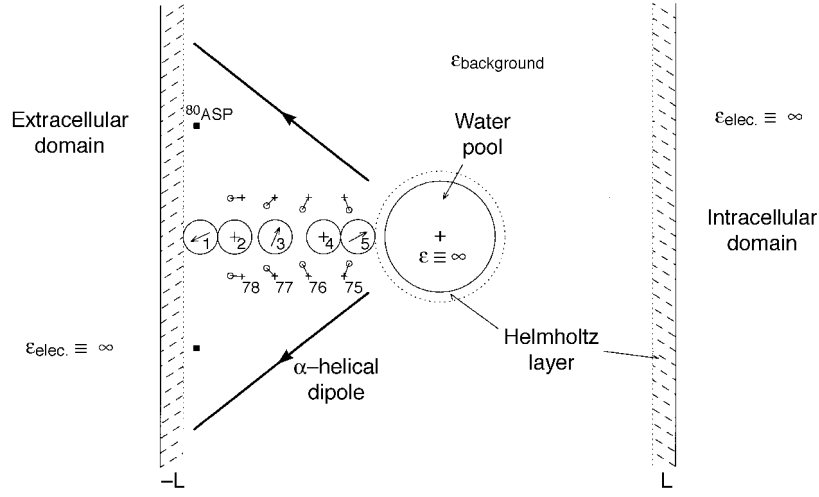

FIG. 1. Semi-microscopic model geometry for the KcsA selectivity filter. It includes solvating CO groups (residues 75–78 of each tetramer strand), single file ions and waters, peptide dipoles, the ^{80}Asp carboxylates, the aqueous cavity and its included ion. Bulk electrolyte and the cavity are treated as dielectric continua, $\varepsilon \equiv \infty$. The Helmholtz layer (accounting for water immobilized by interaction with polar surfaces) separating the explicit sources in the filter from extracellular bulk water has a width of 2 Å; that between the filter and the mid-channel water pool is 1.5 Å. The pool radius is 5.0 Å and it accommodates $\sim$20 waters. The crystallographic occupancy sites (2 and 4) are $\sim$18.5 Å and $\sim$11.0 Å from the cavity centre.

mobile, reorientable moieties in the low ε dielectric background. The surrounding membrane and those parts of the channel not explicitly modelled form a background continuum dielectric with ε_{back}, ~ 2. The picture is semi-quantitative, designed to deconstruct individual structural features' influences on ion transfer and to facilitate comparison of ion–channel interactions among the alkali cations.

This approach permits description of the proximate structural reorganizations associated with ionic solvation in a channel environment; exactly treating charge induced dielectric relaxation of 'solvent', i.e. the parts of the system nearest the transported ion(s). The choice of $\varepsilon_{back} \sim 2$ derives from the index of refraction (the high frequency dielectric constant); it is the electronic contribution to ε. This approach circumvents drawbacks of both Poisson–Boltzmann and Brownian treatments where the constriction is treated as a high ε continuum, even though it contains ordered, non-permittive single-file waters (Partenskii & Jordan 1992, Partenskii et al 1994) and where all protein charges are immobile, with stabilization arising from (real) structural reorganization dealt with by assigning the protein an elevated effective ε, between 4 and 20 (Antosiewicz et al 1994, Gibas & Subramaniam 1996).

In our treatment, structural reorganization of the single file waters and the binding pocket carbonyls in the ions' immediate vicinity is treated exactly; other electrical features are stationary. The model is fundamentally electrostatic; channel solvation involves transfer of an ion into a cavity accompanied by dielectric reorganization of the immediate surroundings. The approach is very efficient computationally. With $\sim$80–100 mobile sources, statistically reliable free energy perturbation calculations for any point on the permeation pathway are achieved in $\leqslant$10 h on a personal computer. Model parameters roughly reproduce alkali metal hydration energies and gross aspects of both ion–water and water–water pair correlation functions.

Permeation is a composite process. The ion is **dehydrated**, and exchanged for water in the gas phase; the ion is transferred to a **cavity** in the background dielectric and exchanged for water; it is then **stabilized** by exchange for a water molecule in the channel:

$$\text{Ion(aq)} + \text{Water(vac)} \rightarrow \text{Ion(vac)} + \text{Water(aq)} \qquad \text{Dehydration} \quad (1a)$$

$$\text{Ion(vac)} + \text{Water}(\varepsilon_{back}) \rightarrow \text{Ion}(\varepsilon_{back}) + \text{Water(vac)} \qquad \text{Cavity} \quad (1b)$$

$$\text{Ion}(\varepsilon_{back}) + \text{Water(channel)} \rightarrow \text{Ion(channel)} + \text{Water}(\varepsilon_{back}) \qquad \text{Stabilization} \quad (1c)$$

The stabilization energy is computed by perturbation methods described previously (Dorman et al 1996); the dehydration energy is experimentally

accessible[1]; the cavity term is a Born energy, determined by the ion's cavity radius in the channel.

The model of Fig. 1 has five sites. Four have crystallographic correspondences (Doyle et al 1998) and/or rough electrophysiological identifications (Neyton & Miller 1988): sites 2 and 4 are the crystallographic sites (outer lock-in and enhancement respectively); site 3 is the interionic water site; and site 5 approximates the Ba block site (Jiang & MacKinnon 2000). The extracellular boundary site 1, identified from simulational studies, more or less accounts for extracellular vestibular water's influence on filter energetics. Default geometry is a strand-averaged symmetrization of the crystallographic coordinates. For computational efficiency carbonyl carbons are immobilized, a restriction that can be lifted. Oxygens rotate about the carbons, weakly tethered to equilibrium orientations determined by minimizing the crystallographic structure with an unoccupied filter (hypothetical). Waters and ions are not constrained. In default geometry the cavity, of ~ 5 Å radius, is centred 26 Å and 23 Å from the extra- and intracellular boundaries, respectively. The temperature is 300 K.

Role of the cavity

The cavity's major role is to stabilize an ion near the centre of the membrane (Doyle et al 1998, Roux & MacKinnon 1999). However, does it also help stabilize ions in the selectivity filter? Or might it have some other secondary influence on permeation? Is proximity to the cavity as effective as bulk water in stabilizing filter ions; if not, how large is the penalty? Does the cavity isolate the filter from the low ε domain on the channel's intracellular side? Are filter energetics very different in the open channel? Is the cavity as effective in stabilizing filter ions as additional single file waters?

Tables 1–3 provide answers to these questions, by limiting consideration to ion–water interaction. Five basic variants from default geometry of Fig. 1 are treated: (1) replace the cavity by explicit waters; (2) vary cavity radius, at constant overall system width; (3) approximate an open state, shrinking overall system width until the cavity contacts the intracellular region or (4) deforming the cavity to a tube contacting the intracellular region and filled with explicit waters; and (5) eliminate the cavity, replacing it by additional single file waters.

[1]The process of Eq. 1a is hypothetical, but energies can be estimated with a fair degree of confidence. What is needed is the absolute potential of the standard hydrogen electrode. The most recent experimental and theoretical determinations differ by ~ 7 kT (Reiss & Heller 1985; Tissandier et al 1998); dehydration free energies are thus uncertain to ± 3.5 kT.

TABLE 1 Effect of cavity size and cavity occupancy (cases 1 and 2, see text) on monovalent ion stabilization free energies (Eq. 1c, in kT) for single occupancy of the model filter (Fig. 1, the default geometry)

	Width/Å	R_{cavity}/Å	*Explicit waters*	*Site 1*	*Site 2*	*Site 3*	*Site 4*	*Site 5*
Default	49	5	File-5, Cavity-0	−28.3	−25.8	−20.5	−20.4	−19.2
Case 1	49	5	File-5, Cavity-20	−28.1	−25.4	−20.4	−20.7	−20.6
Case 2	49	8.5	File-5, Cavity-0	−28.4	−26.0	−21.0	−21.6	−21.9
Case 2	49	0	File-5, Cavity-0	−28.0	−25.2	−19.8	−18.7	−14.7

Case 1 replaces the continuum cavity by explicit cavity water (see text).

TABLE 2 Effect of varying intracellular channel geometry (cases 3 and 4, see text) on monovalent ion stabilization free energies (Eq. 1c, in kT) for single occupancy of the model filter (Fig. 1, the default geometry)

	Width/Å	R_{cavity}/Å	*Explicit Waters*	*Site 1*	*Site 2*	*Site 3*	*Site 4*	*Site 5*
Default	49	5	File-5, Cavity-0	−28.3	−25.8	−20.5	−20.4	−19.2
Case 3	33	5	File-5, Cavity-0	−28.6	−26.2	−21.2	−21.5	−21.1
Case 4	49	Tube	File-5, Tube-72	−28.4	−25.7	−20.8	−21.7	−22.3

Case 4 incorporates explicit 'tube' water (see text).

TABLE 3 Effect of replacing the continuum cavity by single file waters (case 5, see text) on monovalent ion stabilization free energies (Eq. 1c, in kT) for single occupancy of the model filter (Fig. 1, the default geometry)

	Width/Å	R_{cavity}/Å	*Explicit waters*	*Site 1*	*Site 2*	*Site 3*	*Site 4*	*Site 5*
Default	49	5	File-5, Cavity-0	–28.3	–25.8	–20.5	–20.4	–19.2
Case 5	49	0	File-5, Cavity-0	–28.0	–25.2	–19.8	–18.7	–14.7
Case 5	49	0	File-6, Cavity-0	–28.1	–25.6	–20.5	–20.5	–21.8
Case 5	49	0	File-7, Cavity-0	–28.2	–25.8	–20.8	–21.4	–23.6
Case 5	49	0	File-8, Cavity-0	–28.3	–25.9	–21.1	–22.0	–24.5

Stabilization energies at site 1, furthest from the cavity, are, as expected, essentially independent of intracellular structure, suggesting an overall statistical uncertainty of ± 0.3 kT.

Table 1 describes different modifications of the cavity: filling it with explicit waters (case 1) or varying its radius (case 2). The inclusion of explicit cavity waters tests the high ε, continuum cavity approximation. But for site 5, adjacent

to the cavity, there are no major differences[2]. Altering the cavity radius noticeably perturbs ionic stability at the two inner sites; the effect is moderate at site 4 ($\sim$kT) and large ($\geqslant$2 kT) only at the innermost site, 5.

Table 2 illustrates the effect that transition to an open state may have on filter energetics. Whether the continuum cavity contacts the intracellular space (case 3) or the water-filled cavity is extended and connected to the intracellular space (case 4), outer site energetics is unaltered. Again changes at site 4 are small, but real ($\sim$kT) and those at site 5 are moderate ($\sim$2–3 kT).

Table 3 contrasts the influence of the cavity on filter ion stabilization with that of hypothetical additional single file waters. One single file water would be fully compensatory.

A clear picture emerges. Not surprisingly, the cavity isn't designed with an eye toward filter energetics; additional single file waters would be more effective. It clearly helps stabilize ions at site 5; since ion–cavity interactions arise from image forces, quadratically dependent on valence, they may contribute to Ba stabilization near the channel–cavity boundary. The cavity electrically isolates filter ions from the non-permittive intracellular side of the channel assembly. Without a change in filter geometry, filter energetics could only be marginally altered in the transition from closed to open state.

Ion transfer energetics — individual electrical features and stabilization

As an ion enters the channel, ion–protein interaction must offset the ion's dehydration energy. The solvation environment along the interior of the permeation pathway is dramatically different from that in bulk water. The dehydration energy (Eq. 1a) ranges from 115 (Cs^+) to 160 (Na^+) kT. This is balanced by cavity (Eq. 1b) and stabilization (Eq. 1c) components. We first focus on stabilization, the process occurring within the uniform dielectric background; at each site it is roughly the same (to within $\sim$15 kT) for the four alkali cations and compensates for 50–65% of the dehydration energy.

Deconvolution of ionic interaction with individual structural features provides insight into how each helps make the filter ionophilic. We consider (hypothetical) single occupancy and separately assess the influence of bulk and cavity water, of the single file waters, of the binding pocket carbonyls, of the oriented α helices, and of the ^{80}Asp near the extracellular mouth. Figures 2 and 3 decompose the stabilization free energy for one K^+-like ion in the filter. They illustrate each feature's

[2]This may overestimate the cavity's stabilizing ability. MD simulation of water in $\sim$20 Å cavities suggests an ε of $\sim$5 (Zhang et al 1995), like that in single file channels (Partenskii & Jordan 1992, Partenskii et al 1994). However, work on large cylindrical channels (radius $\sim$8 Å) is consistent with a larger ε, $\sim$30 (Sansom et al 1997).

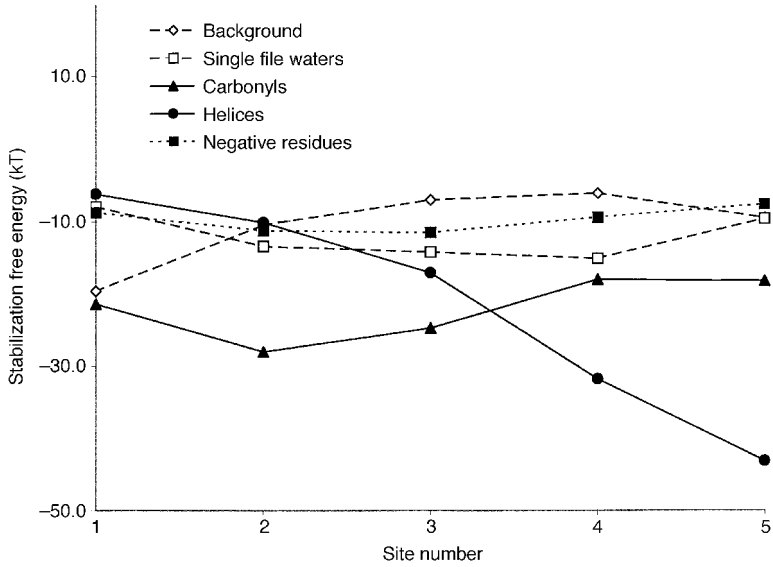

FIG. 2. Individual contributions of the various electrical features (continuum background, ◇; single file waters, □; binding pocket carbonyls, ▲; oriented α helices, ●; negative residues, ■) to monovalent ion stabilization energy at various occupancy sites in the model KcsA filter. The cavity is unoccupied.

contribution to the stabilization free energy (Eq. 1c), for scenarios where the cavity is ion free (Fig. 2) or occupied (Fig. 3) by a monovalent cation. For K^+, the total stabilization energy at the physiological sites (2–5) ranges between 75 and 85 kT.

Consider ionic stabilization with the cavity ion free (Fig. 2). Attraction to the dielectric background (bulk and cavity water) is strongest near the two boundaries; the cavity is half as effective as bulk water. Stabilization by the single file waters is complementary, weakest at the boundary sites where the ion has but one single file neighbour. Net interaction with waters of all kinds (bulk, cavity and single file) varies from ~20 to ~30 kT. The remaining dielectric stabilization mainly reflects ion–carbonyl and ion–helix attraction. Near the cavity the filter sites are very near the α helices' C-termini and helix interaction dominates. The C-termini are ~6 Å from sites 4 and 5 but ~14 Å from site 2; in all cases the amino termini are ~20 Å away. The ^{80}Asp at the peptide–water interface are strongly shielded by nearby bulk solvent; their ability to stabilize filter cations is consequently much reduced[3].

[3]In the dielectric picture, each of these charges induces an electrical image (of opposite polarity) in the solvent, creating a dipole. Near the aqueous interface these charge separations are small; their influence on ions in the selectivity filter is much less than that of effective dipoles created by charged groups in the low ε interior.

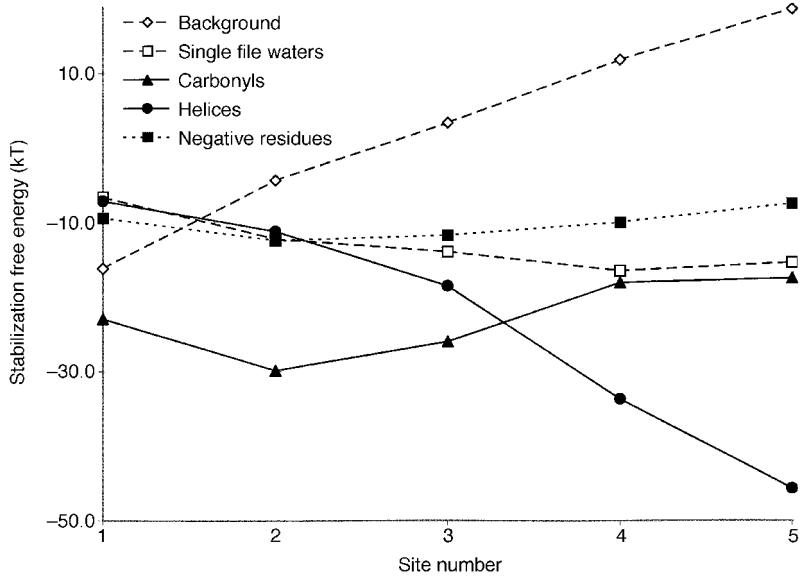

FIG. 3. Individual contributions of the various electrical features (continuum background, ◇; single file waters, □; binding pocket carbonyls, ▲; oriented α helices, ●; negative residues, ■) to monovalent ion stabilization energy at various occupancy sites in the model KcsA filter. The cavity is occupied by a monovalent cation.

Introducing an ion into the cavity (Fig. 3) has little effect on ion–peptide energetics. Interaction with the background (here including the cavity ion) destabilizes the filter ion; interionic repulsion decreases much more rapidly than R^{-1} due to solvent (image) effects. Ions at site 2 or 3 are much closer to the cavity ion's (negatively charged) image than are ions at site 4 or 5; net filter ion–cavity ion repulsion at site 2 is ~35% that at site 4, even though their direct coulombic interaction is ~60% as large. At site 5 there is significant compensation. Interaction with the single file water becomes relatively favourable since the cavity ion reinforces a site 5 ion's tendency to align channel water.

Ion transfer energetics — the ionic Born cavity

Processes (a) and (b) of Eq. 1 require charge transfer between different dielectrics. Experimental data provide reliable estimates for step (a), dehydration (see footnote 1). Step (b) is a Born transfer from vacuum to the uniform background ($\varepsilon_{back} = 2$); the associated energy is

$$\Delta G_{Born} = \tfrac{1}{2}(1/\varepsilon_{background} - 1)q^2/R_{cavity} \qquad (2)$$

TABLE 4 Ion–oxygen distances (in Å) in an energy minimized KcsA K^+ channel for alkali cations occupying the crystallographic sites (2 and 4). Bold face entries are for oxygens identified as forming part of the binding cavity boundary

	Binding site 2				*Binding site 4*			
Ion	*W–1*	*O–78*	*O–77*	*W–3*	*W–3*	*O–76*	*O–75*	*W–5*
Na^+	**2.40**	**3.69**, 4.24, 5.00, 4.75	**2.38**, **2.47**, **2.36**, **2.47**	**2.29**	5.63	4.26, **3.83**, 4.53, 4.64	**2.28**, **2.31**, **2.32**, **2.38**	**2.34**
K^+	**2.60**	4.86, 3.77, 4.78, **3.14**	**2.64**, **2.69**, **2.66**, **2.68**	**2.72**	3.48	**2.70**, **2.75**, **2.91**, **2.82**	**2.67**, **2.76**, **2.75**, **2.67**	3.98
Rb^+	**2.86**	3.95, **3.33**, 5.07, **3.29**	**2.75**, **2.85**, **2.80**, **2.73**	**2.71**	3.62	**2.83**, **2.88**, **2.79**, **2.73**	**2.86**, **2.90**, **2.78**, **2.81**	3.60
Cs^+	**2.98**	3.51, 3.72, **3.37**, 5.16	**2.92**, **2.93**, **3.02**, **2.91**	**2.86**	**3.05**	**2.95**, **3.06**, **2.97**, **3.02**	**3.07**, **2.99**, **3.04**, **2.96**	3.69

W–1 is the distance from the ion to the water oxygen at site 1, etc. O–78 is the distance from the ion to the carbonyl oxygens of residues 78, etc.

The cavity radius, R_{cavity} is determined by establishing a dividing surface separating ion from 'solvent'. This distance is not an intrinsic ionic property; it is also solvent dependent (Grunwald 1997). This is especially true in the non-uniform, inherently non-symmetric medium (even when time averaged) of a channel interior (Jordan 2002). In principle, the ion could ideally associate unconstrained single file waters. However, the binding pocket carbonyl oxygens are significantly constrained, their range of motion limited by the peptide backbone's rigidity (Doyle et al 1998, Bernèche & Roux 2000). At each of sites 2–4 the oxygens from eight carbonyl and two single file waters form the binding environment. However, not all coordinate the permeant ion equally well. In addition, different ions are more or less effectively coordinated. Table 4 presents ion–oxygen distances for energy-minimized channels containing a single alkali cation at sites 2 and 4. The rest of the filter, the cavity and the extracellular vestibule are filled with water. The local environments are far from symmetric; only some ligands form part of the first solvation shell. To estimate the size of the cavity, we proceed somewhat arbitrarily, assuming (1) that at least one carbonyl from each set of ligands must form a part of the boundary and (2) that waters are not necessarily bounding ligands. Thus, at site 2 mean distances between ions and their bounding ligands are 2.58 Å for Na^+, 2.73 Å for K^+, 2.83 Å for Rb^+ and 3.00 Å for Cs^+. While mean ion–oxygen distances for the larger alkali cations are nearly optimal (similar to those in water), that for Na^+ is very large. The Na^+–K^+ difference is only 0.15 Å, much less than in water, 0.38 Å; the channel does not adjust as well to Na^+ as to the other alkali cations. Consequently the Born energy,

TABLE 5 Decomposition of ion transfer free energy (in kT) for alkali cations occupying the crystallographic sites (2 and 4) of a singly occupied channel (with ion-free cavity)

	Binding site 2				*Binding site 4*			
Ion	Na^+	K^+	Rb^+	Cs^+	Na^+	K^+	Rb^+	Cs^+
Dehydration	163.1	134.3	125.2	115.9	163.1	134.3	125.2	115.9
Cavity	−98.8	−86.9	−74.8	−70.3	−100.5	−84.3	−78.1	−69.7
Stabilization	−76.1	−73.9	−73.0	−69.7	−86.2	−81.7	−81.8	−76.7
Total	−11.8	−26.5	−22.5	−24.1	−22.7	−31.7	−34.7	−30.5

Eq. 2, is relatively small for Na^+. To quantitate the cavity energy requires an estimate of the size of the O atom; as we are using energy minimized structures to estimate cavity size, we choose a rather small value for the O atom radius, 1.3 Å, consistent with recent *ab initio* studies (Roux & Karplus 1995).

Ion transfer energetics — summary

Table 5 presents the individual contributions to the free energy of ion transfer from water to the channel interior for alkali cation occupancy of sites 2 and 4. Due to our approximations, total free energies are highly approximate. The results are most useful for contrasting filter interaction among the alkali cations. Cavity and stabilization components are comparable. Both the electrostatic interaction (stabilization) and the cavity contribution are largest for Na^+. This ion interacts extremely well with the peptide, better than its larger congeners, consistent with the suggestion that internal Na^+ blocks K^+ permeation (Heginbotham et al 1999). However, as the peptide is insufficiently flexible, the Na^+ cavity remains too large; the net interaction is inadequate to fully compensate for Na^+'s much larger dehydration energy.

Figure 4 presents estimates of the ion transfer free energies, relative to K^+ at site 2, for alkali cation occupancy of the crystallographic sites[4]. Na^+ occupancy is always unfavourable. On average it is $\sim$15 kT less stable than K^+, comparable with observed permeability ratios that imply a $\Delta G \sim 10$ kT (Hille 1992). While the larger alkali cations are energetically similar, Cs^+ clearly interacts less well

[4]Sites 1 and 5 are both eliminated from consideration, the former because it really is not part of the single file, the latter because the explicit solvation environment is incomplete. States with ions occupying neighbouring sites are energetically inaccessible and thus ignored.

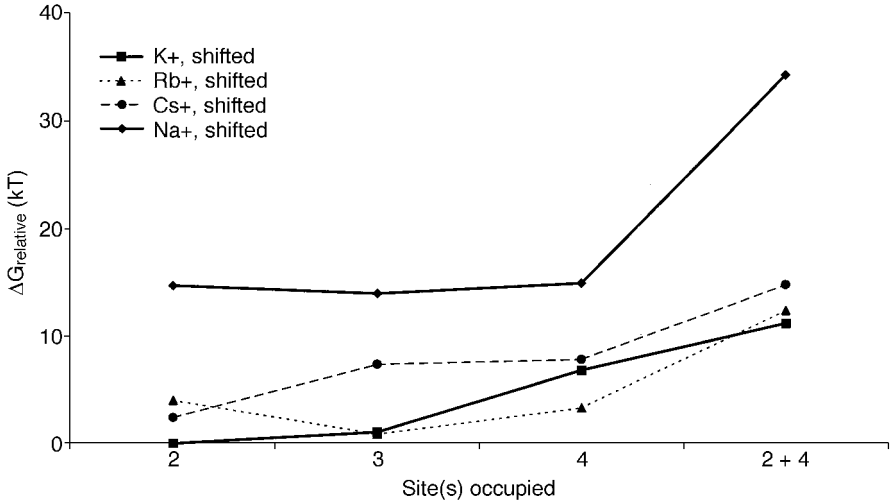

FIG. 4. Permeation free energy, relative to K^+ occupancy of site 2, for single and double alkali cation occupancy of four states of the selectivity filter of the model KcsA channel (Na^+,◆; K^+, ■; Rb^+, ▲; Cs^+, ●). All energies have been displaced by +52.6 kT; the shifted free energies are independent of the cavity's ionic occupancy state.

than either K^+ or Rb^+; there appears to be a slight preference for K^+ over Rb^+. Both observations are consistent with experiments.

Model limitations

This approach to permeation energetics is highly approximate. Significant terms, like the energy required to create an uncharged Born cavity, have been ignored (Roux et al 1990). Dielectric relaxation has been limited to the ions' first solvation shell; other structural features were immobilized. The outer vestibule and the cavity are viewed as low and high ε dielectric continua respectively. These are all restrictions that can be lifted.

Conclusions

Even in its limited form, this model provides a way to separately assess how individual architectural features of the channel affect permeation. It demonstrates that the cavity effectively isolates the filter from the intracellular domain and that it is especially effective in aiding stabilization of divalent ions at the cavity–filter boundary (the Ba-block site). It demonstrates that the oriented α helices, in addition to stabilizing an ion in the cavity, also contribute importantly to ionic stabilization at the cavity–filter boundary. It corroborates the idea that peptide

rigidity may be at the heart of K^+ channel selectivity (Doyle et al 1998). It demonstrates that discrimination among the larger alkali cations requires delicate energetic trade-offs involving Born stabilization in the dielectric cavity and dielectric stabilization by the surrounding charge distribution.

Acknowledgements

This work supported by the National Center for Supercomputing Applications and by the National Institutes of Health, grant GM-28643. We thank M. B. Partenskii for helpful comments. D. Patangia determined the data of Table 4.

References

Antosiewicz J, McCammon JA, Gilson MK 1994 Prediction of pH-dependent properties of proteins. J Mol Biol 238:415–436

Åqvist J, Luzhkov V 2000 Ion permeation mechanism of the potassium channel. Nature 404:881–884

Bernèche S, Roux B 2000 Molecular dynamics of the KcsA K^+ channel in a bilayer membrane. Biophys J 78:2900–2917

Biggin PC, Smith GR, Shrivastava I, Choe S, Sansom MSP 2001 Potassium and sodium ions in a potassium channel studied by molecular dynamics simulations. Biochim Biophys Acta 1510:1–9

Chang G, Spencer RH, Lee AT, Barclay MT, Rees DC 1998 Structure of the McsL homolog from *Mycobacterium tuberculosis*: A gated mechanosensitive ion channel. Science 282:2220–2226

Chiu SW, Jakobsson E, Subramaniam S, McCammon JA 1991 Time-correlation analysis of simulated water motion in flexible and rigid gramicidin channels. Biophys J 60:273–285

Chung S-H, Allen TW, Hoyles M, Kuyucak S 1999 Permeation of ions across the potassium channel: Brownian dynamics studies. Biophys J 77:2517–2533

Dorman VL, Partenskii MB, Jordan PC 1996 A semi-microscopic Monte Carlo study of permeation energetics in a gramicidin-like channel: the origin of cation selectivity. Biophys J 70:121–134

Dorman VL, Garofoli S, Jordan PC 1999 Ionic interactions in multiply occupied channels. In: Gramicidin and related ion-channel forming peptides. Wiley, Chichester, (Novartis Found Symp 225) p 153–169

Doyle DA, Morais-Cabral J, Pfuetzner RA et al 1998 The structure of the potassium channel: Molecular basis of K^+ conduction and selectivity. Science 280:69–77

Fu D, Libson A, Miercke LJ et al 2000 Structure of a glycerol-conducting channel and the basis of its selectivity. Science 290:481–486

Gibas CJ, Subramaniam S 1996 Explicit models in protein pK_a calculations. Biophys J 71:138–147

Grunwald E 1997 Thermodynamics of molecular species. Wiley-Interscience, New York

Guidoni L, Torre V, Carloni P 2000 Water and potassium dynamics inside the KcsA K^+ channel. FEBS Lett 477:37–42

Heginbotham L, LeMasurier L, Kolmakova-Partensky L, Miller C 1999 Single *Streptomyces lividans* K^+ channels: functional asymmetries and sidedness of proton activation. J Gen Physiol 114:551–560

Hille B 1992 Ionic channels of excitable membranes, 2nd edn. Sinauer Associates, Sunderland, MA

Hille B, Schwartz W 1978 Potassium channels as multi-ion single-file pores. J Gen Physiol 72:409–442

Jakobsson E, Chiu SW 1987 Stochastic theory of ion movement in channels with single-ion occupancy. Application to sodium permeation of gramicidin channels. Biophys J 52:33–45

Jiang Y, MacKinnon R 2000 The barium site in a potassium channel by X-ray crystallography. J Gen Physiol 115:269–272

Jordan P 2002 Ionic energetics in narrow channels. In: Layton H (ed) Proceedings of the IMA Workshop on Membrane Transport and Renal Physiology. Springer-Verlag, New York, in press

Murata K, Mitsuoka K, Hirai T et al 2000 Structural determinants of water permeation through aquaporin-1. Nature 407:599–605

Neyton J, Miller C 1988 Discrete Ba^{2+} block as a probe of ion occupancy and pore structure in the high conductance Ca^{2+}- activated K^+ channel. J Gen Physiol 92:569–586

Partenskii MB, Jordan PC 1992 Theoretical perspectives on ion channel electrostatics. Continuum and microscopic approaches. Q Rev Biophys 24:477–510

Partenskii MB, Dorman V, Jordan PC 1994 Influence of a channel-forming peptide on energy barriers to ion permeation, viewed from a continuum dielectric perspective. Biophys J 67:1429–1438

Reiss H, Heller A 1985 The absolute potential of the standard hydrogen electrode: A new estimate. J Phys Chem 89:4207–4213

Roux B, Yu H-A, Karplus M 1990 Molecular basis for the Born model of ion solvation. J Phys Chem 94:4683–4688

Roux B, Karplus M 1994 Molecular dynamics simulations of the gramicidin channel. Annu Rev Biophys Biomol Struct 23:731–761

Roux B, Karplus M 1995 Potential energy function for cation-peptide interactions: An *ab initio* study. J Comp Chem 16:690–704

Roux B, MacKinnon R 1999 The cavity and pore helices in the KcsA K^+ channel: electrostatic stabilization of monovalent cations. Science 285:100–102

Sansom MS, Smith GR, Adcock C, Biggin PC 1997 The dielectric properties of water within model transbilayer pores. Biophys J 73:2404–2415

Shrivastava IH, Sansom MS 2000 Simulations of ion permeation through a potassium channel: molecular dynamics of KcsA in a phospholipid bilayer. Biophys J 78:557–570

Tissandier MD, Cowan KA, Feng WY et al 1998 The proton's absolute enthalpy and Gibbs free energy of solvation from cluster-ion solvation data. J Phys Chem A 102:7787–7794

Wallace B 1999 X-ray crystallographic structures of gramicidin and their relation to the *Streptomyces lividans* potassium channel structure. In: Gramicidin and related ion-channel forming peptides. Wiley, Chichester (Novartis Found Symp 225) p 23–37

Woolf TB, Roux B 1997 The binding of sodium in the gramicidin A channel: comparison of molecular dynamics with solid-state NMR data. Biophys J 72:1930–1945

Zhang L, Davis HT, Kroll DM, White HS 1995 Molecular dynamics simulation of water in a spherical cavity. J Chem Phys 99:2878–2884

DISCUSSION

Tieleman: How do you treat the energy differences between the ions in vacuum and the ions in water?

Jordan: We have a background dielectric constant of two. We have a three point model for water and we have adjusted things so that in terms of our thermodynamic cycle we can come within 3–5 kT of the dehydration energies.

The radii are reasonably well tuned. My Na^+ is 1 Å, K^+ is 1.3 Å, Rb^+ is 1.5 Å and Cs^+ is 1.7 Å: with these I come within about 3 kT of the dehydration energies determined experimentally.

Roux: How do you calculate the dehydration energy?

Jordan: We make up a sphere about 15 Å in diameter that has a bunch of our model waters in it. We go through the whole equivalent cycle and do the calculations.

Roux: Do you correct for what is beyond 15 Å?

Jordan: Yes, but it is an imperfect approach, even for establishing parameters. We must estimate the size of the cavity that surrounds the ions. This is even more of a problem in our modelling of KcsA since the carbons of the carbonyls are immobile, so we can't in any consistent way determine the size of the cavities surrounding the ions. The cavity sizes we used have therefore been derived rather differently. We have just minimized the structures using molecular mechanics and looked at how the immediate surroundings of the ions at the various sites differ as the ion is varied. It is really cobbled together at that point, which is why the numbers are screwy. This is one of the reasons we really want to let those carbons move so that we have an internally consistent picture.

Roux: With regard to the ion solvation problem, I don't doubt that it is possible to calibrate a potential function by doing the free energy calculation with the ions. Nonetheless, when you start to look at the literature, it is very disconcerting that the solvation free energy of these simple cations and chloride is uncertain, in fact well beyond the selectivity of biological channels. A recent discussion of the large variations in ion solvation can be found in Pliego & Riveros (2000). The estimate for the free energy of Na^+ ranges from -92 to -100 kcal/mol, and for Cl^- it ranges from -78 kcal/mol to -86 kcal/mol. Then all of a sudden Cl^- is very close to Na^+, whereas I always thought it was close to K^+. There is no way the computational people will be able to do anything meaningful until those numbers are tied down.

Jordan: People have been working on this problem for a long time. The problem comes down to getting an absolute electrode potential for the hydrogen electrode.

Roux: Isn't it possible to choose something else as a reference?

Jordan: It doesn't make any difference. If you had an absolute measurement of the hydrogen electrode it would be fixed. Every time this unknown parameter is changed, you move all the monovalent cations up an amount and all the monovalent anions down by the same amount. With the divalents whatever happens is doubled.

Sansom: Does that change the relative position within the monovalent cations?

Jordan: No, but it drastically alters cation and anion values. Among the more recent values, there was an experimental determination of the standard hydrogen electrode potential by Reiss & Heller (1985) that was about 7 kT different from an

extrapolated procedure done very recently, based on the idea that if you think about adding waters to the ion microclusters, you will eventually get a solvated ion (Tissandier et al 1998). This is for free energy. If you are interested in enthalpy of solvation, it is even worse.

Roux: With improvements in technology is there any hope that a better measurement could be made?

Jordan: No, because ultimately you are doing a measurement that requires you to come up with some way of approximating what is happening in the interface. One of the ways of dealing with this is to try to find how much of a potential change occurs when you bring the ion directly across the interface. This is very hard to do. People have worked on this and come up with different ways of doing it. If I had to guess I would say that there is an uncertainty of about $\pm 3.5\,kT$. These numbers differ from Marcus's estimates (Marcus 1991) by about $50\,Kj\,mol^{-1}$, mainly because we use a different value for the absolute potential of the standard hydrogen electrode. But there is also another problem. If you look at the numbers he quotes in his tables and then go back to your freshman chemistry texts and work through the relative free energies for the alkali cations, the numbers aren't completely internally consistent. He has cobbled things together and made some approximations of his own. It is a real problem.

Sansom: If you had a slightly more deformable cavity, do you think one could switch the exact value of the K^+ versus Na^+ selectivity? That is, would there be smaller ΔG if you allowed more deformability in the cavity?

Jordan: I would imagine that if things were more deformable, the ΔGs of permeation would mush together. It depends on the root-mean-square displacements that I assign to the carbon motion. In our experiments the cavity radii were determined in a way that makes things roughly comparable to what people have determined using molecular dynamics.

Sansom: At the back of my mind are channels such as Kir6.2, where the tyrosine of the filter is replaced by a phenylalanine and the Na^+/K^+ selectivity is lower.

Jordan: We can certainly adjust the model to give more mobility to the waters in the cavity. Until now we have been dealing with a spherical cavity, because this is a historical artefact. We introduced this because when one does continuum electrostatics it is easy to compete with a spherical cavity. If we are putting explicit waters in there (which doesn't cost us very much), we could change the shape of the cavity. We could probably also give the cavity walls some flexibility.

Perozo: I am trying to come to terms with your numbers and calculations in the sense of a working channel. You calculate ion flux. What kind of single-charge currents do you get?

Jordan: I can't do it. If I look at what I have here, if I solve for conductance using these free energies I would find values of absolutely zero.

Perozo: Then, in any calculation based on the KcsA structure, do people get energies compatible with the single-charge currents that have been mentioned? That is, do people get something comparable to what would make sense given the actual conductances?

Roux: To get the correct magnitude of flux, you don't expect free energy barrier of more than 3 or 4 kcal/mol.

Perozo: So what are the values that people have obtained based on the structure?

Roux: It depends whether you allow the structure to be flexible or not. If you keep the structure very rigid, you will get one kind of answer. If you allow the full dynamics of the structure, you get a fairly different kind of answer.

Perozo: What I am really getting at is that you try to come to ways such that your terms make sense from the physical character point of view. Could it be that the structure used in the calculations is not the right one?

Jordan: That is possible. I am stuck with what the experimentalists give me.

Roux: According to our calculations, the selectivity filter of the X-ray structure can sustain a flux. There is no big free energy barrier with that structure, and as far as we can tell the activity filter is not in a 'closed' state.

Sansom: You should be able to test this. You could apply different levels of restraint to the X-ray structure, from rigid to soft restraints allowing a very large distortion. We know that if it is held rigid the barriers will be too great to sustain the observed flux, so imagine letting it soften more and more, and then determine at what stage the free energies become compatible with the experimental flux. I don't think you have to allow it to change greatly, but some deformability is needed.

Perozo: It is clear that it doesn't need to be a great change. It cannot change that much because it is surrounded by all the transmembrane helices. The question is, to what extent do we let it change?

Sansom: Despite the reservations one might have about simulations, we have seen a degree of flexibility in terms of things such as a flip round the valine of one of the carbonyls, for example (Shrivastava & Sansom 2000). We would expect some deformability of those carbonyls to track the ions as they move through the channel. Benoit Roux, have you calculated PMFs (potentials of mean force) with different degrees of rigidity of the filter?

Roux: That is not quite how we did it, but there are certainly indications that the flexibility of the selectivity filter is important. For example, the Tyr78 (of the GYG signature sequence) is forming a hydrogen bond with Trp68 in the crystallographic structure. If the hydrogen bond is made artificially stronger by applying an energy restraint, then the free energy barriers for ion conduction are increased. What is remarkable is that this hydrogen bond is nearly 12 Å away from where the ions are located, even though it has an impact on ion conduction. This is an example of a very delocalized and long-range effect from flexibility. It is certain that the

flexibility of the protein will affect the free energy barriers controlling ion conduction.

Ashcroft: What happens in your simulations if you stick an F in there rather than a Y?

Roux: We haven't done this, since it would weaken the hydrogen bond; it would probably flatten the free energy profile.

Unwin: My understanding is that the flux of K^+ through the KcsA channel isn't nearly as high as with some K^+ channels, and also the selectivity is not as good. Has anyone got any insights as to what to do to the channels to make them more selective and flux at a higher rate?

Perozo: Depending on the permeant ion concentration, KcsA has a conductance as high as most channels, and it is also quite selective. It is just like any other K^+ channel.

Unwin: So the design is absolutely optimized for flux and selectivity.

Perozo: Yes. There are many K^+ channels that conduct poorly compared with KcsA.

Sansom: Peter Jordan, going back to your breakdown of terms at the different sites, and accepting all these reservations about absolute magnitudes, if we add all those terms up, does it look flat or do you see preference for certain sites within the filter?

Jordan: If it is singly occupied, I see a preference for ion occupancy of the water site. This is my site 3. I dropped consideration of the two external sites because, in both those cases, the environment is part explicit solvent and part continuum solvent. If I have two ions in the filter, there is only one occupancy possibility because you are not going to have the two ions at neighbouring sites.

Sansom: Can you break down ΔG to ΔH and $T\Delta S$? Could you look at how things would change from room temperature to crystallographic temperature?

Jordan: Yes.

References

Marcus Y 1991 Thermodynamics of solvation of ions. Part 5. Gibbs free energy of hydration at 298.15 K. Faraday Soc Trans I 87:2995–2999

Pliego JR, Riveros JM 2000 New values for the absolute solvation free energy of univalent ions in aqueous solution. Chem Phys Lett 332:597–602

Reiss H, Heller A 1985 The absolute potential of the standard hydrogen electrode: a new estimate. J Phys Chem 89:4207–4213

Shrivastava IH, Sansom MSP 2000 Simulations of ion permeation through a potassium channel: molecular dynamics of KcsA in a phospholipid bilayer. Biophys J 78:557–570

Tissandier MD, Cowan KA, Feng WY et al 1998 The proton's absolute enthalpy and Gibbs free energy of solvation from cluster-ion solvation data. J Phys Chem 102:7787–7794

Ion Channels: From Atomic Resolution Physiology to Functional Genomics: Novartis Foundation Symposium 245. Volume 245
Edited by Gregory Bock and Jamie A. Goode
 ISBN: 0-470-84375-6

Index of contributors

Non-participating co-authors are indicated by asterisks. Entries in bold indicate papers; other entries refer to discussion contributions.

A

Ashcroft, F. 49, 63, 81, 82, 103, 126, 142, 144, 158, 159, 165, 166, 191, 192, 203, 206, 218, 219, 220, 221, 259, 261, 264
Auerbach, A. 48, 103, 106, 168, **223**, 234, 235, 236, 237, 238

B

*Baker, K. A. **169**
*Beckstein, O. **66**
*Biggin, P. C. **66**
*Bond, P. **66**
*Brejc, K. **22**

C

*Cheng, A. **33**
Choe, S. 18, 19, 20, 30, 31, 49, 61, 62, 63, 64, 65, 80, 82, 83, 105, 142, 143, 144, 158, 163, 165, 166, 167, **169**, 175, 176, 177, 205
Corringer, P.-J. 16, 18, 19, 82, 159, 238, 258, 259
*Cortes, D. M. **146**
*Cuello, L. G. **146**
*Culetto, E. **240**
*Cushman, S. **169**

D

*Dorman, V. L. **109**
Doyle, D. 47, 61

F

*Faraldo-Gómez, J. **66**
Findlay, J. B. C. **207**, 218, 219, 220, 221
*Franks, C. **240**
*Froger, A. **33**
Fu, D. 20, 30, 49, **51**, 61, 62, 63, 64, 162, 163, 166, 204, 235, 237, 257

G

*Garofoli, S. **109**
*Grauso, M. **240**
*Grigorieff, N. **193**
Gulbis, J. M. 32, **127**, 142, 143, 144, 176

H

*Harrison, M. A. **207**

J

Jordan, P. C. 18, 48, 62, **109**, 122, 123, 124, 125, 126, 234, 235

L

Lambert, J. 15, 18, 259
*Law, R. J. **66**
*Libson, A. **51**
*Lin, M. A. **178**
*Liu, Y.-S. **146**

M

Mathie, A. 17, 32, 50, 81, 143, 177
Miller, K. 17, 18, 19, 20, 31, 48, 81, 82, 107, 165, 166, 167, 168, 175, 205, 218, 219, 221, 258, 259, 262, 263
*Miloshevsky, G. **109**

Mindell, J. A. 17, 29, 48, 49, 61, 63, 80, 81, 102, 104, 105, 106, 107, 143, 158, 160, 166, 191, **193**, 203, 204, 205, 206, 261, 262, 263, 264
Mitra, A. K. 19, **33**, 46, 47, 48, 49, 50, 61, 63, 64, 160, 192, 205, 262

P

Papazian, D. M. 19, 64, 102, 104, 105, 142, 144, 175, **178**, 190, 191, 192, 261, 263
*Patargias, G. **66**
Perozo, E. 16, 17, 19, 31, 47, 64, 79, 83, 103, 104, 105, 124, 125, 126, **146**, 158, 159, 160, 161, 162, 163, 165, 166, 190, 203, 205, 261, 264
*Pfaffinger, P. **169**
*Pirruccello, M. M. **193**

R

*Raymond, V. **240**
*Reddy, V. S. **33**
*Ren, G. **33**
Roux, B. 15, 17, 31, 63, 79, 80, 81, **84**, 101, 102, 103, 104, 105, 106, 107, 123, 124, 125, 126, 161, 192, 219, 221, 235, 236, 237, 261, 263, 264

S

Sansom, M. S. P. **1**, 17, 20, 32, 49, 50, 61, 62, **66**, 79, 80, 81, 82, 83, 102, 103, 104, 105, 107, 123, 124, 125, 126, 144, 159, 160, 165, 166, 190, 204, 205, 219, 220, 221, 237, 257, 260, 262, 263
Sattelle, D. B. 30, 50, **240**, 257, 258, 259, 260
Schirmer, T. 220
Schrempf, H. 30, 48, 49, 64, 80, 143, 158, 162, 176, 219, 220, 258
*Silverman, W. R. **178**
Sixma, T. K. 16, **22**, 29, 30, 31, 32, 79, 104, 162, 238
*Smit, A. B. **22**
*Sompornpisut, P. **146**
*Stroud, R. **51**
Swartz, K. 101, 102, 105, 106, 142, 143, 159, 163, 191, 204, 205, 206, 264

T

*Tang, C. Y. **178**
Tieleman, D. P. 21, 46, **66**, 122
*Tiwara-Woodruff, S. K. **178**
*Towers, P. **240**

U

Unwin, N. **5**, 15, 16, 17, 18, 19, 20, 21, 31, 47, 49, 79, 82, 126, 160, 161, 166, 175, 204, 205, 206, 219

V

*van Dijk, W. J. **22**

W

Wallace, B. A. 29, 63, 175, 204

Ion Channels: From Atomic Resolution Physiology to Functional Genomics: Novartis Foundation Symposium 245. Volume 245
Edited by Gregory Bock and Jamie A. Goode
 ISBN: 0-470-84375-6

Subject index

A

acetylcholine-binding protein (AChBP) 16, 22–29, 223, 231, 233
  α subunit 24–25
  binding sites 30
  δ subunit 25
  disulfide bonds 24
  evolutionary origin 31–32
  ψ subunit 25
  homopentamer 23
  immunoglobulin fold 23–24
  loop regions 25–26
  toxin binding 29
  tyrosine cornerstone 24
acetylcholine-gated channel 5–15
  ACh-binding pockets 6, 16
  α helical segment 7, 8, 9
  α subunits 6, 16
    rotation 12, 18
  anion channels 247–248
  basic architecture 5-7
  charge distribution 15
  disulfide bonds 18, 19
  framing residues 8
  gate 6, 9
  gating action 10, 12, 20
  hydrophobic residues 9
  ion-conducting pathway 6
  leucine residues 9, 12
  M2 8, 9, 10, 12, 20
  M4 18
  MA 7–8
  mutagenesis experiments 12–13, 17
  pore
    closed 8–9
    constriction zone 6
    open 9–10, 17
  vestibules 6–7
    cytoplasmic 7–8, 19
    extracellular 7
    role 7–8
  windows 7–8, 18
acetylcholine receptors (AChRs) 223–234
  gating 223, 224–225
    spatial organization 230
  genomics 240–257
    propagation 230–231
    rate–equilibrium linear free energy 227–233, 234–235, 23
    structure 223–224
ACh-binding pockets 6, 16
acr-2 245
acr-3 245
acr-4 245
ACR-7 246
ACR-8-like group 245
acr-16 245
ACR-16-like group 245–246, 258–259
ACR-16 subunit 249–250
AgTx2 103, 106, 263
alamethicin 68
aldicarb 247
aldo-keto reductase (AKR) superfamily 128
  β subunit, relationship to 131–134
α barrel structures 53
α helical segments 7, 8, 9
α subunits 6, 16, 24–25
  rotation 12, 18
Alzheimer's disease, drug management 241
amino acid sequencing 1
amphipathic channels 54, 71
antimonite permeability 52
antisense approach, neural signalling 254
AQP1 *see* aquaporin 1
AQP2 50
AQPZ 52
  channel permeability and selectivity 52, 54
  ion exclusion 55
aquaglyceroporins 51, 52
  conservation 56–59, 61
  obesity and 52
aquaporin 1 (AQP1) 33–46, 109
  α barrels 53
  aqueous passage 38, 40, 42
    diffusion-limited 34

aquaporin 1 (AQP1) (*cont.*)
binding sites 43
carbon dioxide permeability 34
cation conductance 34, 42
conservation 56, 61
constricted region 110
density map 35
electron crystallographic data 36
fourfold axis region 42–43, 47, 49
gating 50
hydrophobic residues 42, 43, 48, 49
monomer halves, spatial disposition 38
mutagenesis experiments 34
N- and C-terminals 35, 38
NPA loop 34, 38
polar residues 42, 48
pores 38, 40, 42, 47
quasi-twofold symmetry 53
structure 52–53, 71
aquaporins 51, 52
channel-lining residue mutations 50
conservation 56–59, 61
correlated mutation analysis 263
physiological significance 52
water molecule behaviour in 71–73
Arg187 50
Asn76 43, 48
Asn192 43, 48

B

bacteriorhodopsin 47
β subunit 127–142, 173, 177
catalytic activity 129, 131
cell surface expression 128
channel inactivation 128
historical context 128–129
octamer 129, 134, 143–144
redox activity 129, 142
relationship to AKRs 131–134
T1–β assembly 134–137, 142
T1–S1 linker 137–140
tertiary fold 128, 131–134
Born energy 113, 117, 118–119
Brownian dynamics 110–111
bungarotoxin 250
binding 29
butamisole 250

C

Caenorhabditis elegans 241
antisense approach, neural signalling 254
calcium imaging 253
channel diversity, reasons for 257–258
electrophysiology 253
gene silencing 254
as a genetic model 242
nicotinic receptors 250–251
protein diversity 260
subunit spatial expression patterns 246
calcium imaging 253
carbon dioxide permeability 34
cardiac action potential 191
cation conductance 34, 42
cavity 111–112, 170
permeation energetics 117–119
radius 118
role 113–115
charge distribution 15
chloride channels, monovalent anion selectivity 204 *see also* ClC-type chloride channels
choline 224, 250
ClC-type chloride channels, electron diffraction 193–203
data analysis 195
diffraction patterns 199, 201
projection structure 201–202
specimen preparation 194–195
COMP 9
conformational sampling 94
conservation 27–28, 56–59, 61, 170, 209
correlated mutation analysis 263–264
Cys189 34
Cys-loop 27
Cys-loop receptors 22–23
cysteine scanning mutagenesis 13, 19–20
cytoplasmic vestibules 7–8, 19, 170

D

D_{PORE}/D_{BULK} 68–69
D194 231
D274 188
D278 185, 187
D327 187
DEG-3 245, 250
DEG-3-like group 245, 246
dehydration energy 112, 123

dementia, nAChR reduction 251
DES-2 245, 250
diabetes insipidus, nephrogenic 50, 52
dicydrohexylcarbodiimide 213
dipole–dipole interaction 148, 150
distance energy restraints 92
disulfide bonds 18, 19, 24
double-stranded RNA interference 254
Drosophila melanogaster 241
  as a genetic model 252
  nAChR gene family 252
drug development/targets 1, 241, 242, 245
drug resistance 242

E

E5 214
E152 55–56, 62
E283 182–184
eat-2 245
eat-18 245
egg-laying behaviour, nicotinic receptor genes 251
electron crystallographic data 36
electron diffraction 193–203
  data analysis 195
  specimen preparation 194–195
electron paramagnetic resonance (EPR) spectroscopy 146–158, 159–160, 167
  principles and data 148–150
electrophysiology 253
electrostatics 68, 110–111
epilepsy 241
EriC crystals 194
  electron diffraction 194–202
    data analysis 195
    diffraction patterns 199, 201
    projection structure 201–202
    specimen preparation 194–195
ether-à-go-go (eag) 191
  acidic residues 185, 187–188
  expression 191
  magnesium binding 185, 187–188, 190, 191
  metal ion binding 102
  voltage sensor 180, 184–188
evolution 31–32, 59
extracellular vestibules 7

F

F200 55
F_0 domain 214, 220
F_0F_1-ATPase 215, 218
flicker 159
framing residues 8
Friedel R factors 195–197, 201

G

G199 55
gate/gating 28, 84
  acetylcholine-gated channels 6, 9, 10, 12, 20
  AChR 223, 224–225, 230
  AQP1 50
  current analysis 180
  equilibrium constant 223
  hydrophobic 69–71
  KcsA 154–157, 158–159, 161
  unliganded 238–239
GCN4 leucine zipper 43
gene silencing 254
genomics 2–3, 240–257
glia cells 23
GlpF 42, 43, 49, 51–61, 109
  α barrels 53
  amphipathic channel lining 54, 71
  antimonite permeability 52
  channel permeability and selectivity 52, 54–56
  conservation 56–59, 61
  crossing contacts 56–57
  hydrogen bonding 54–55
  ion exclusion 55–56
  NPA motif 57, 61
  physiological role 63
  polarity 62
  polyol permeability 52, 54
  quasi-twofold symmetry 53–54
  stability 64
  structure 52–54, 71
  vestibules 58
  water in 62, 71–73
Glu140 212
glycerol release 52
glycine stripe 212, 220
glycophorin mutagenesis 261
gramicidin 110
green fluorescent protein 258

Gromacs 69
GROMOS96 69
GxxxG motif 212

H

hanging basket 137
hanging gondola 91, 171
Heisenberg spin exchange 148
HEPES buffer 26, 30–31
HERG 191
His180 43
HOLE 69
hydrogen bonding 54–55
hydrophobic gate 69–71
hydrophobic residues 9, 42, 43, 48, 49
3α-hydroxysteroid-dihydrodiol dehydrogenase (HSD) 131, 133, 134

I

immunoglobulin fold 23–24
interspin distances 148, 150
intragenic suppression 89
ion exclusion 55–56
ion solvation 123
ivermectin 250

J

jtf-38 245, 249

K

K374 181–182
K_v channels 84–85, 127
  conservation 170
  cytoplasmic vestibule 170
  proteins regulating excitability 177
  side openings 170
  T1 domain and excitability 169–175
  tetramerization 170
  voltage sensor 171, 178–190
    function 179
    S2/S4 involvement 180
    two-phase movement 180
K_v1 channel, β subunit 127–142
  catalytic activity 129, 131
  cell surface expression 128
  channel inactivation 128
  historical context 128–129
  octamer 129, 134, 143–144
  redox activity 129, 142
  relationship to AKRs 131–134
  T1–β assembly 134–137, 142
  T1–S1 linker 137–140
  tertiary fold 128, 131–134
KchIP 173, 177
KcsA 2, 109
  cavity 111–112
    permeation energetics 117–119
    radius 118
    role 113–115
  constricted region 109–110
  crystallographic structure 85
  gating mechanism 154–157, 158–159, 161
  hydrophobic gate 70
  mobility 159–160
  permeation energetics 111, 115–120
  pH dependency 154, 162–163
  simulation 79
  site-directed spin labelling 150–154
  structural similarity to Shaker 88–89
  structure 85
kinetic modelling 1
Kubo–Zwanzig Linear Response Theory 81

L

lanthanide-based resonance energy transfer (LRET) 89–90, 92, 94, 101, 107
leucine residues 9, 12
leucine side chains 69–70
LEV-1 251, 258
lev-11 247
levamisole resistance 242, 250
ligand binding 23, 24–25
ligand-gated ion channel superfamily, conservation 27–28
light harvesting complex (LHC) 201
LINCS algorithm 69
lipid-exposed residues 92–94
Lys51 43, 49

M

M2 8, 9, 10, 12, 20
M4 18
MA 7–8
magnesium binding 185, 187–188, 190, 191
McsL 109
  hydrophobic side chains 69–70

mechanosensitive channels 9
membrane proteins 1, 67
N-methyllycaconitine (MLA) 250
MIP members 33–34
MODELLER 92
molecular dynamics 68, 69, 110
Molscript 69
morantel 250
muscle 246, 247
mutagenesis experiments 12–13, 17, 34, 90–91, 261
myasthenias 241

N

nephrogenic diabetes insipidus 50, 52
nervous system development, nAChRs in 246, 251–252
neuronal sprouting 251–252
nicotinamide adenine dinucleotide phosphate (NADP) 129
nicotinic acetylcholine receptor (nAChRs), genomics 240–257
diverse gene family 245–246
drug targets 242, 245
egg laying behaviour 251
functional and pharmacological diversity 249–250
genes functionally linked to 246–247
mutations 241
nervous system development 246, 251–252
novel functions 247–248
nitroxide dynamics 148
Nod26 48, 50
non-liganded receptor opening 238–239

O

O program 35
obesity 52
OmpA 73–76
oxantel 250

P

patch clamping 1
permeation energetics 111, 115–120
perturbations 225
pH dependency 154, 162–163
pharyngeal muscle activity 245, 251
Φ 226, 228, 229–232, 233, 235, 236, 237, 238–239
phospholamban 9
PME 69
Po–V relationship 180
polar residues 42, 48
polyol permeability 52, 54
pores
AQP1 38, 40, 42, 47
blocking 90
closed 8–9
constriction zone 6
models 68, 92
open 9–10, 17
openness 70–71
Shaker 88–89, 92
typical 67
power saturation 148
proline 20
proteolipid
16 kDa 209, 210–212
conservation 209
proton channel *see* vacuolar H^+-ATPase
pyrantel 250

Q

Q–V relationship 180, 191
quaternary ammonium pore blocker 90
QX222 12

R

R206 55–56
R factors 195–197, 201
RasMol 69
Raster3d 69
rate–equilibrium linear free energy (LFER) 225–233, 234–235, 236
redox activity 129, 142
residue environmental phase diagram 151
restraint-driven Cartesian transformation (ReDCaT) 155
rhodopsin 262
ribitol 54, 55
ric-3 247
RNA editing 177

S

S1–S4 87–88, 91
S2, voltage sensing 84–85, 180

S4 94, 95–96, 97, 101, 102, 104, 188
voltage sensing 85, 180
scanning mutagenesis 90–91
schizophrenia, drug management 241
second site suppressor analysis 181–184, 190–191
Shaker 84–101
central pore 88–89, 92
conformational sampling 94
distance energy restraints 92
intragenic suppression 89
lanthanide-based resonance energy transfer (LRET) 89–90, 92, 94, 101, 107
lipid-exposed residues 92–94
modelization 91–92
pore blocking 90
S1–S4 87–88, 91
S4 94, 95–96, 97, 101, 102, 104, 188
scanning mutagenesis 90–91
simulated annealing 94
structural similarity to KcsA 88–89
two-domain architecture 91
voltage sensor 85, 179, 181–184
side chain associations 97
SIGMAA 35
simulated annealing 94
single-molecule spectroscopy 166
site-directed spin labelling 146
KcsA 150–154
solvent accessibility 148
solvent-accessible surface area (SASA) 93
spectral second moment 148
spin label I 146–147
spin label dynamics (mobility) 148, 159–160
spin labelled molecules, structural information from 148
Src kinase 177
stabilization energy 112
synaptogenesis 246

T

T1 128, 169–175
cavity 170
conformational changes 171–172
physiological role 171–172
removal 175
voltage-sensing 171
zinc binding 171, 173, 176
T1–β assembly 134–137, 142, 170, 171
T1–S1 linker 137–140
tandem dimer constraints 155
temperature 234–235
threonine 12
TIM barrel 129, 133
tin derivative 213–214
Tourette's syndrome, drug management 241
toxin binding 29
tropomyosin 247
tryptophan scan 105
twitchin 247
tyrosine cornerstone 24

U

unc-22 247
UNC-29 246, 251, 258
UNC-29-like group 245, 249
unc-38 251
UNC-38-like group 249
unc-50 246
UNC-63 258
UNCL 246–247
unliganded gating 238–239

V

vacuolar H^+-ATPase 207–218
16 kDa proteolipid 209, 210–212
functionally sensitive sites 212–214
mechanism of action 215–216
transmembrane organization 209–210
valines 9
vestibules 6–7, 58
cytoplasmic 7–8, 19, 170
extracellular 7
role 7–8
VMD 69
voltage gating 139–140
voltage sensor 171, 178–190
function 179
S2/S4 involvement 84–85, 180
two-phase movement 180
Vph1p 210, 214–215, 218

W

water 66–78
behaviour
AQP1 34, 38, 40, 42
GlpF 62, 71–73
binding, AQP1 43
dynamic behaviour 68

electrostatic properties 68
models 68, 69
windows 7–8, 18

X

X-ray crystallography 52
XPLOR 35
xylitol 54, 55

Z

zinc binding 171, 173, 176